International Journal of Thermal Sciences 181 (2022) 107742

Contents lists available at ScienceDirect

International Journal of Thermal Sciences

journal homepage: www.elsevier.com/locate/ijts

An electron–phonon Monte Carlo study on thermal transport in GaN

Anish Muthukunnil Joseph, Bing-Yang Cao *

Key Laboratory of Thermal Science and Power Engineering, Ministry of Education, Department of Engineering Mechanics, Tsinghua University, Beijing 100084, China

ARTICLE INFO

Keywords:
Boltzmann transport equation
Electron–phonon interaction
Electron–phonon Monte Carlo
Polar optical potential
Deformation potential

ABSTRACT

Heat conduction in micro/nano-scale materials are well modeled by Boltzmann transport equation (BTE) and the Monte Carlo (MC) method is an effective computational tool for solving BTE. In conventional insulators and semiconductors, phonons are the majority heat carriers and contribution of electron–phonon interaction (EPI) is negligible. However, in polar semiconductors electron–phonon interaction and its contribution to thermal conductivity are significantly high. In this paper, we develop a novel MC scheme which combines phonon and electron transport effectively to address electron–phonon interaction (EPI). The method is applied in a case study, simulating the thermal transport in wurtzite Gallium Nitride (GaN), considering the EPI impact into account. Deformation potential as well as polar optical potential (POP) are used to characterize EPI. Individual scattering rates of electrons are first determined. Using them the net scattering rate and relaxation times are calculated. Both lattice temperature and the electron temperature profiles in the computational domain are estimated and compared. The final inference is that the lattice thermal conductivity of wurtzite GaN at room temperature is found to be reduced by 16%–22%, on incorporating EPI, for samples of varying thicknesses.

1. Introduction

Electrons and phonons are the major carriers of thermal energy in solids [1]. While electrons have a dominant contribution to the thermal conductivity in metals, phonons play a significant role in semiconductors and insulators. Over the past few decades, rapid advancements in first-principles simulation and thermal metrology have caused to an elaborate understanding of the thermal transport properties of electrons and phonons. On the computational side, simulation methods based on density functional theory (DFT), density functional perturbation theory (DFPT), and phonon Boltzmann transport equation (BTE) are frequently used to compute the thermal conductivities of crystalline materials which are limited by phonon–phonon, phonon–impurity, and phonon–boundary scatterings [2]. Recent studies by Feng and Ruan [3] have improved the phonon–phonon scattering calculation by including the higher-order four-phonon scattering processes. These calculations have a good agreement with experimental results and can resolve individual phonon modes' contribution to thermal transport. On the experimental side, recent developments of the phonon mean-free-path spectroscopy [4,5] have given rise to detailed information of thermal transport contribution from phonons with different mean free paths. Among all the scattering processes of phonons, the electron–phonon interaction (EPI) has been thoroughly studied for its impact on electrical transport properties, including electrical resistance and superconductivity. However, its significance in thermal transport started to be appreciated only recently [6].

Initially, the efforts were merely focused on the influence of EPI on the properties of electrons in metals and semiconductors, including the explanations for the temperature dependence of electrical conductivity and electronic thermal conductivity. And, very less attention was given to the lattice thermal conductivity, or the thermal conductivity governed by phonons, since in metals, it is generally believed that phonon contribution to thermal conductivity is negligible compared to the electronic counterpart. Since thermal conduction is dominated by phonons in semiconductors, the impact of EPI on phonon transport receives less attention due to relatively low carrier concentrations, which limits the scattering of phonons by electrons much less important than the phonon–phonon scattering. The first study on this regard was done by Sommerfeld and Bethe [7], they calculated the relaxation time of phonons incorporating EPI in metals. Based on that, Makinson [8] proposed an expression for the lattice thermal conductivity of metals as a function of temperature, where he concluded that the electrons interact equally with longitudinal and transverse phonons, different from Bloch's coupling scheme [9] that restricts the electrons only interact with longitudinal phonon modes.

It was only recently the development of first-principles calculations for phonon–phonon [10,11] and electron–phonon interactions [12]

* Corresponding author.
E-mail addresses: aneshmj@gmail.com (Anish M.J.), caoby@tsinghua.edu.cn (B.-Y. Cao).

https://doi.org/10.1016/j.ijthermalsci.2022.107742
Received 6 November 2021; Received in revised form 29 May 2022; Accepted 7 June 2022

Nomenclature

β	Phonon–Impurity scattering probability
ϵ_0	Permittivity of free space
$\hbar$	Planck constant
κ	Effective thermal conductivity
ω	Phonon frequency
τ	Relaxation time
B_{3ph}	3-Phonon relaxation parameter
B_I	Impurity relaxation parameter
D	Phonon density of states
D_O	Coupling constant
$E(k)$	Electron energy
e	electron charge
E_c	Conduction band energy
$F(r)$	Electric field
f	Fermi distribution
f_0	Equilibrium Fermi distribution
F_{ei}	Cumulative electron number density
F_i	Cumulative phonon number density
$g(E)$	Electron density of states
H'	Perturbation Hamiltonian
k	Electron momentum vector
K_0	Static dielectric constant
K_∞	High frequency dielectric constant
k_B	Boltzmann constant
L_D	Debye length
l_e	Electron mean free path
M	Matrix element
m^*	Electron effective mass
n	Phonon distribution
n_{De}	Net electron density
n_{Dp}	Net phonon density
N_I	Impurity density
N_i	Number of Phonons per unit volume
P	Probability
q	Phonon momentum vector
r	Random number
S	Electron scattering probability
T	Temperature
t	Electron–Phonon density ratio
T_e	Electron temperature
u	Lattice displacement
V	Lattice volume
v_d	Electron drift velocity
v_g	Phonon group velocity
v_s	Sound velocity
v_{th}	Electron thermal velocity
Z_A	Acoustic deformation potential
Z_O	Optical deformation potential

that the effect of EPI on phonon transport is thoroughly evaluated in a variety of materials, demonstrating the thermal conductivity in solids can be strongly modified by the scattering of phonons by a high concentration of electrons [6], and the change of the phonon frequencies (“re-normalization”) caused by EPI. The effect of EPI on phonon transport has been analyzed in several heavily doped materials through studies of their dependence of lattice thermal conductivity on carrier concentration. Moreover, recent studies on the thermal conductivity of metals have shown that in certain transition metals, the lattice thermal conductivity is found to be non-negligible compared with the electronic thermal conductivity [13]. Ankit Jain et al. [14] presents Density functional theory and lattice dynamics calculations to predict Mode-dependent phonon and electron transport properties in Al, Ag, and Au. They predicted thermal conductivities, electrical conductivities, electron–phonon coupling coefficients and electron–phonon mass enhancement parameters are in agreement with experimental measurements. At a temperature of 100 K, the phonon contribution to the total thermal conductivity of Al is 5% in bulk and increases to 15% for a 50 nm thick film. At 300 K, phonon contribution to thermal conductivity in Al, Ag and Au were estimated to be 2.4%, 1% and 0.71% respectively.

This work builds upon the previous studies on MC phonon transport as well as MC electron transport [15–27]. In 1988, in order to interpret the results from thermal conductivity experiments at low temperatures, Klitsner et al. developed the first phonon Monte Carlo, without considering internal scattering mechanisms that were unimportant due to the long phonon mean free path at low temperature [28]. In 1994, Peterson [29] formulated a Monte Carlo simulation that included phonon–phonon scattering using the relaxation-time approximation. Since that time, a number of notable advancements have been made, including dispersion relation incorporation [23–30] frequency-dependent relaxation times, scattering sub-step energy conservation, periodic boundary conditions, and variance-reduced formulations.

In this work, as a case study, the lattice thermal conductivity of GaN is calculated using a step by step electron–phonon MC algorithm, taking all types of scattering scenarios into account. The electron MC runs side by side with the phonon tracing MC [15] resulting the electron–phonon MC. The MC simulation solves the BTE in a statistical methodology and has been widely used to simulate radiative transfer, electron and hole transport in semiconductors [16–20]. A large number of articles which use MC technique for phonon transport have been published in the past few decades [21–25]. However, implementing MC technique for studying EPI and its impacts on the lattice thermal conductivity, are not really addressed so far, which is the main scope of this work. Gallium Nitride (GaN) is a polar semiconductor with wide band gap (E_g=3.39 eV) and high mechanical stability. It has made path breaking advancements in many areas such as light emitting diodes (LEDs), opto-electronics and high frequency electronics [31,32]. Heat dissipation and management are still challenging issues in GaN based devices. Thermal conductivity is the ability of a material to conduct heat and majority of the semiconductors effectively describe it by means of intrinsic phonon–phonon interactions and extrinsic scattering due to ionic impurities or isotopes [33,34]. Previously, Lindsay and co-workers [35] studied the contribution of PPI and isotopic scattering to lattice thermal conductivity in GaN, and inferred a large isotope effect of 60%–65%. In a recent work, Dao-Sheng et al. [36] investigated thermal transport properties of GaN considering the effects from biaxial strain and electron–phonon coupling (EPC) using the first principles calculation and phonon Boltzmann transport equation. Upon incorporating EPC, they reported a reduction in the thermal conductivity of 26.8%, 4.6% and 23.5% for free state, +5% strain state and −5% strain state respectively. Another work by Jia-Yue Yang et al. studied the Fröhlich EPI contribution to the thermal conductivity of GaN. They found that the lattice thermal conductivity of GaN is reduced by 24%–34% [37] after incorporating EPI. A lot more past works on thermal conductivity of GaN can be found in the Table 1. Our main objective is to present an algorithm for studying phonon transport side by side with electron transport which is then applied on GaN to understand the heat transport mechanisms beyond the intrinsic phonon–phonon interactions (PPI).

Table 1
A list of past studies on thermal conductivity of GaN.

Author	Year	Method	Reported thermal conductivity
Jia-Yue Yang et al. [37]	2016	First principle (DFT)	250-200 W/mK; 250-315 K
Dao-sheng Tanget al. [36]	2020	First principle (DFT)	188 W/mK; 300 K
Guangzhao Qing et al. [38]	2017	First principle (DFT)	180-70 W/mK; 150-500 K
Masaru Kmano et al. [39]	2002	Photo-thermal divergence	170-140 W/mK; 200-400 K
V. M. Asnin et al. [40]	1999	STM	170-140 W/mK; 200-400
Elbara Ziad et al. [41]	2015	FDTR	150-75 W/mK; 300-600 K
C. Mion et al. [42]	2017	3-Omega	134-139 W/mK; 300 K
Tahakiro Kawamura et al. [43]	2005	Molecular Dynamics	310-75 W/mK; 300-1200 K
X. W. Zhou et al. [44]	2012	Molecular Dynamics	185-74 W/mK; 300-800 K
Qiye Zheng et al. [45]	2019	Thermo reflectance	380-40 W/mK; 150-850 K
C. Luo et al. [46]	2001	3-Omega	500-150 W/mK; 50-400 K

2. Electron–phonon Monte Carlo method

In an MC simulation technique, point particles (such as electrons, phonons, holes etc.) are drawn, distributed in the computational domain and let evolve in time. Individual trajectories of the particles are tracked by imposing various scattering mechanisms.

2.1. Phonon Monte Carlo

It is widely accepted to use BTE for describing particle transport, which in the absence of an external force takes the form [47],

$$\frac{\partial n}{\partial t} + v_g \nabla n = \left[\frac{\partial n}{\partial t}\right]_{scat}, \tag{1}$$

where v_g is the group velocity, n is the distribution function and right-hand side represents the rate of change of n due to scattering. Phonon tracing MC algorithm [15] is used in this work where phonon BTE is solved under the relaxation time approximation, thereby computational particles describe only deviation from the equilibrium distribution. Phonon tracing MC cuts down the computational time significantly in comparison with phonon ensemble MC [26]. First MC is run without gray media approximation, considering phonon dispersion relations into account, to calculate the average values of mean free path, frequency, relation time, group velocity etc. of individual phonon bundles. Second, MC under gray media approximation, is run along with electron MC to study the EPI and other scattering processes and their impacts on thermal transport. In this study, phonon dispersion relations are obtained from "Brillouin zone boundary condition"(BZBC) model proposed by Chung et al. [48]. The relaxation time formulations by Holland [49] are also used.

Energy of each phonon bundle is directly related to the frequency by, $E(\omega) \propto \hbar\omega$. Hence initializing the frequency would, by default, sets the energy too. As a first step, the maximum (cut off) frequencies for LA and TA branches are determined as ω_{LAmax} and ω_{TAmax}. The frequency space between zero and maximum is discretized into N_b intervals (N_b = 40 for this study). The number of phonons per unit volume in the i_{th} spectral interval is given by [23],

$$N_i = \sum_{p=1}^{2} n(\omega_i, p) D(\omega_i, p) \triangle \omega_i, \tag{2}$$

where n is the Bose–Einstein function,

$$n = \frac{1}{e^{\frac{\hbar\omega}{k_B T}} - 1}. \tag{3}$$

$D(\omega, p)$ is the phonon density of states. The net phonon number density n_{Dp} is derived as,

$$n_{Dp} = \sum_{i=1}^{N_b} \sum_{p=1}^{2} n(\omega_i, p) D(\omega_i, p) \triangle \omega_i. \tag{4}$$

In order to assign the frequency, a normalized cumulative number density function is constructed as [23],

$$F_i = \frac{\sum_{k=1}^{i} N_k}{\sum_{k=1}^{N_b} N_k}. \tag{5}$$

A random number r is drawn. If $F_{i-1} < r < F_i$, then the phonon belongs to ith interval. Phonon polarization is assigned using the scheme provided in Ref. [24].

Role of optical phonons in the heat transport is negligible as their group velocities are very low compared to LA and TA modes. However, they play a very active and dominant role in interacting with electrons thereby causing an indirect impact on the temperature distribution and the thermal conductivity. And we know that LO phonons in wurtzite GaN eventually decay into a large wave vector TO and LA/TA phonon branches [50,51]*ie.* LO⟶ TO+LA or LO⟶ TO+TA, the resulting LA/TA phonons are then tracked successfully. Typical lifetime of LO phonons in GaN is about 3–4 ps at room temperature [50].

2.1.1. Scattering relaxation times

For the lattice part, only 3-Phonon scattering, Umklaap (U) scattering and Impurity scattering are addressed. Four phonon scattering is negligible for lower temperatures. Hence, it is assumed that role of four phonon scattering in the thermal transport in GaN is negligible. The phonon scattering by impurities is characterized by the relaxation time [24]

$$\frac{1}{\tau_I(\omega, p)} = B_I \omega^4, \tag{6}$$

where B_I is the impurity relaxation parameter and is sensitive to the dispersion model and the group velocities. And for the three phonon scattering, the Umklaap (U) process and normal (N) process are the two modes of intrinsic phonon scattering [24]. Useful expressions given straight forward as,

For N process,

$$\frac{1}{\tau_N(\omega, p)} = \begin{cases} B_{3ph}(p)\omega^2 T^3, & \text{for } LA \\ B_{3ph}(p)\omega^2 T^4, & \text{for } TA \text{ and } \omega < \omega_{\frac{1}{2}} \\ 0, & \text{for } TA \text{ and } \omega \geq \omega_{\frac{1}{2}} \end{cases} \tag{7}$$

For U process,

$$\frac{1}{\tau_U(\omega, p)} = \begin{cases} B_{3ph}(p)\omega^2 T^3, & \text{for } LA \\ B_{3ph}(p)\omega^2 \sinh(\frac{\hbar\omega}{k_b T}), & \text{for } TA \text{ and } \omega \geq \omega_{\frac{1}{2}} \\ 0, & \text{for } TA \text{ and } \omega < \omega_{\frac{1}{2}} \end{cases} \tag{8}$$

B_I, B_{3ph} are determined by standard fitting procedure [24]. Using the above equation effective relaxation time τ_p is written as,

$$\frac{1}{\tau_p} = \frac{1}{\tau_I} + \frac{1}{\tau_U} + \frac{1}{\tau_N}. \tag{9}$$

Deciding which scattering to be undergone is achieved as follows. First, the probability of impurity scattering (β) is calculated using [24],

$$\beta = \frac{\tau_I^{-1}}{\tau_I^{-1} + \tau_{3ph}^{-1}}. \tag{10}$$

Then a random number r is drawn and compared with β. If $r < \beta$, impurity scattering, otherwise three phonon scattering occurs. Impurity scattering is accounted by assigning a new random direction to the incident phonon, assuming isotropic impurity distribution. Else, for three phonon scattering, the phonon is absorbed and track of its path is stopped.

2.2. Electron Monte Carlo

It is a semi-classical MC approach of simulating semiconductor transport [52]. Assuming the carrier motion consists of free flights interrupted by various scattering mechanisms, a computer may be used to simulate the trajectories of particles (electrons) as they move across the device under the influence of an external electric field, using classical mechanics. The scattering events and the duration of particle flight is determined using random numbers. The method is equivalent to solving BTE for electrons.

2.2.1. Theoretical background

BTE for electrons takes the form

$$\frac{\partial f}{\partial t} + \frac{1}{\hbar}\nabla_k E(k)\nabla_r f + \frac{eF(r)}{\hbar}\nabla_k f = \left[\frac{\partial f}{\partial t}\right]_{coll}, \tag{11}$$

where f is the electron distribution, E is the energy, e is the electron charge, $F(r)$ is the external field. In this work, $F(r)$ is taken to be zero. However, a noticeable thermal electro motive force (TEMF) always exists between the hot and cold ends of the sample. The effect of TEMF in modifying the energy of electrons in GaN is estimated to be negligible. Therefore, BTE takes the form,

$$\frac{\partial f}{\partial t} + \frac{1}{\hbar}\nabla_k E(k)\nabla_r f = \left[\frac{\partial f}{\partial t}\right]_{coll}. \tag{12}$$

Under relaxation time approximation BTE further modifies into,

$$\frac{\partial f}{\partial t} + \frac{1}{\hbar}\nabla_k E(k)\nabla_r f = \frac{f - f_0}{\tau_e}, \tag{13}$$

where f_0 is the equilibrium distribution and τ_e is the effective relaxation time for electrons.

Electronic band structure. Parabolic energy bands are assumed for this work. In case of GaN, $E(k)$ is given by,

$$E(k) = \frac{\hbar^2}{2}\left[\frac{k_l^2}{m_l^*} + \frac{2k_t^*}{m_t^2}\right], \tag{14}$$

where m_l^* and m_t^* are longitudinal and transverse effective masses respectively (for GaN $m_l = 0.2m_0$, $m_t = 0.2m_0$)

Scattering mechanisms. A computationally efficient approach to include scattering in MC is to store and use individual scattering rates obtained using Born approximation. Fermi golden rule gives, to the first order, the transition probability per unit time for a scattering from a state $|k\rangle$ to a state $|k'\rangle$ as [52],

$$S(k,k') = \frac{2\pi}{\hbar}|\langle k|H'|k'\rangle|^2.\delta(E - E'), \tag{15}$$

where H' is the perturbation Hamiltonian, E and E' are the initial and final energies. δ is the Dirac Delta function, ensuring the conservation of energy. $\langle k|H'|k'\rangle$ are the matrix elements. The scattering rate summed over all k' yields the probability per unit time to scatter from a state k to any other states in the reciprocal space. And it takes the form,

$$\lambda(k) = \sum_{k'} S(k,k'). \tag{16}$$

In order to get a complete understanding over the scattering processes, one has to consider all such scattering rates $\lambda_1, \lambda_2, \lambda_3, \ldots, \lambda_n$, then, the total scattering rate is given by,

$$\lambda_{tot} = \sum_{i=1}^{n} \lambda_i. \tag{17}$$

The probabilistic direction of scattered particle in three dimensions is given by,

$$P(\theta,\phi)d\theta d\phi = \frac{\sin\theta d\theta d\phi}{4\pi};\ P(\theta) = \frac{\sin\theta}{2};\ P(\phi) = 1/2\pi. \tag{18}$$

The two spherical angles can then be chosen, by generating two random numbers $0 < r_1, r_2 < 1$ such that

$$r_1 = \frac{\phi}{2\pi};\ r_2 = \left(\frac{1-\cos\theta}{2}\right). \tag{19}$$

Electron–phonon scattering. Electron–phonon scattering is, in fact, a mechanism of energy loss. The mobility of carriers in semiconductors is also influenced by electron–phonon scattering, at least around room temperature. Electron–phonon scattering is a major form of inelastic scattering.

Phonons may be emitted or absorbed by electrons, thereby, changing the phonon wave function and energy as well as the electron wave function and energy. Fig. (1.a) shows a Feynman-diagram of electron–phonon scattering. We can treat the phonon scattering in a usual way using Eq. (15) with certain multiplying factors. These factors arise from the wave function. It is evident that a phonon can be absorbed only if at least one phonon is present. Therefore, the result for phonon absorption as obtained by Eq. (15) has to be multiplied by the average number of phonons that are present in the mode 'q' analogous to impurity scattering being multiplied by the impurity density. The appropriate multiplier [52] is the phonon occupation number N_q:

$$N_q = \frac{1}{exp(\hbar\omega_q/k_bT) - 1}. \tag{20}$$

In Eq. (20)$\hbar\omega_q$ is the energy, strongly dependent on q for acoustic phonons and approximately independent for optical phonons. The multiplication factor for phonon emission rate is $(N_q + 1)$. The emission therefore, is composed of two factors. One independent of phonon occupation number and is termed as spontaneous emission (just as in the case of light). The other is called stimulated emission proportional to N_q because more phonons are emitted if more "stimulating" phonons are present. An important approximation to Eq. (20) for the limit $\hbar\omega_q \ll k_BT$, true for acoustic phonons, whose energy is lower enough, is imposed. It is called equipartition approximation which takes the form

$$N_q \approx \frac{1}{1 - \frac{\hbar\omega}{k_BT} - 1} = \frac{k_BT}{\hbar\omega}. \tag{21}$$

Phonons distort the crystal lattice and can create essentially three types of potential energy changes: the deformation potential, the piezoelectric potential, and the polar optical potential. Among them, the piezoelectric potential is significant only at low temperatures, hence not considered in this work, which, presumably takes place at room temperature. The other two, i.e. Polar optical potential (POP) and deformation potential are the key points of interest in this work.

If the lattice is displaced by u, the energy of the conduction or valance band is changed by [52]

$$\triangle E_c = E_c(a) - E_c\left(a + \frac{du}{dx}a\right);\ \triangle E_c = \left(\frac{dE_c}{da}\right)\frac{du}{dx}. \tag{22}$$

The second expression is obtained using Taylor's expansion. Note that we have implicitly assumed that the lattice displacement u has the same effect as expanding or compressing the whole crystal. This means that this concept will actually work if the phonon wave length spans many lattice constants. In three dimensions the change $\triangle E_c$ is proportional to the volume change which is given in terms of the lattice displacement u is given by [52],

$$\frac{\triangle V}{V} = \nabla.u(r), \tag{23}$$

which is basic to Bardeen's deformation potential theory. Hence,

$$\triangle E_c = V.\frac{dE_c}{dV}\nabla u(r), \tag{24}$$

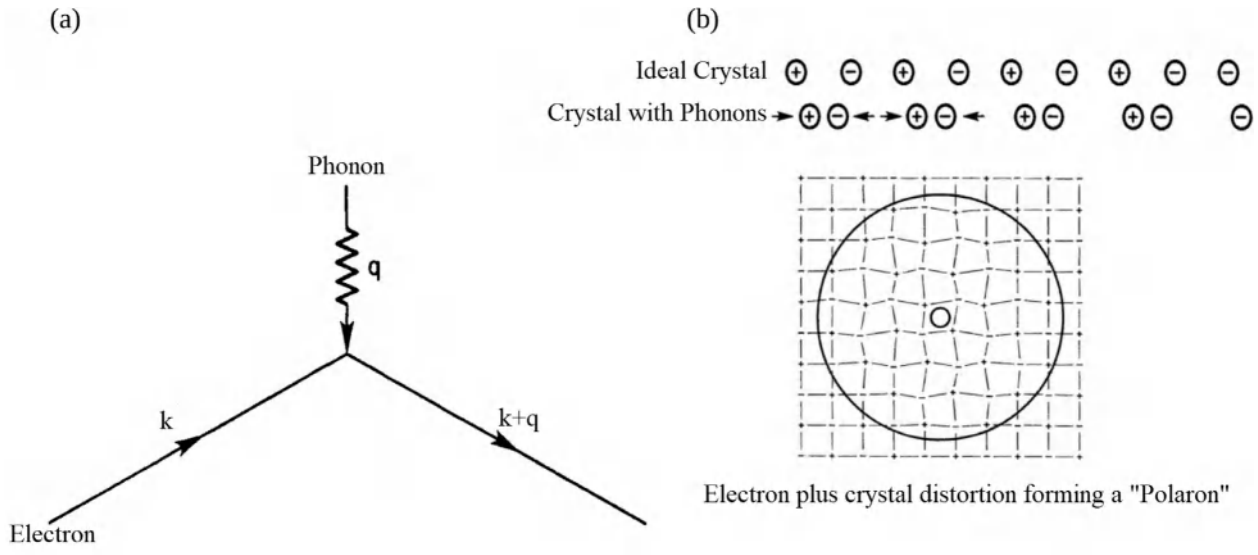

Fig. 1. (a) Schematic of electron–phonon scattering. q, k, $(k+q) \equiv k'$ are the phonon, incident electron and scattered electron wave vectors respectively. (b) A phonon displaces the two sub-lattices of, for example, GaN, against each other. All negative atoms are displaced towards (or away from) the positive atoms.

where, $V.\frac{dE_c}{dV}$ is to be denoted by Z_A, called the acoustic deformation potential. And the perturbing Hamiltonian takes the form,

$$H_A = \triangle E_c = Z_A.\nabla u(r). \tag{25}$$

In general, Z_A has to be replaced by a matrix to account for the anisotropy of crystals and can even depend on the wave-vector.

A typical value for the deformation potential is $Z_A \approx 8$ eV for semiconductor conduction bands and a some-what smaller value for valence bands. We have $u(r)$ of the form [52],

$$u(r) = ue^{iqra};\ k - k' = q, \tag{26}$$

where a is the lattice constant. And the matrix element takes the form [52],

$$M_{k,k'} = \sum_q V_q \delta_{k'-k,q}. \tag{27}$$

Using Eqs. (26) and (27) we have,

$$M_{k,k'} = \pm Z_A iq.u\delta_{k'-k,\pm q} V\left(N_q + \frac{1}{2} \pm \frac{1}{2}\right)^{1/2}. \tag{28}$$

Here we have chosen a plus sign for the q vector in the case of phonon absorption and a minus sign for emission. Notice that transverse waves (wave vector q perpendicular to displacement u) have a vanishing matrix element (the dot product is zero) and therefore do not scatter the electrons. Inserting the value of u in the above equation, the matrix element is rewritten as [52],

$$|\langle k \pm q|H'_A|k\rangle|^2 = \frac{Z_A^2 \hbar\omega_q}{2V\rho v_s^2}\left(N_q + \frac{1}{2} \pm \frac{1}{2}\right). \tag{29}$$

Here V is the volume of the crystal, v_s the velocity of sound, ρ the mass density. The minus sign refers to phonon absorption and the plus sign to phonon emission. The calculation the total phonon scattering rate for LA from the matrix elements requires more algebra and is given by,

$$\lambda_{LA} = \frac{\sqrt{2}}{\pi}\frac{Z_A^2\sqrt{m_l^* m_t^{*2}}k_b T}{\rho\hbar^4 v_s^2}\sqrt{E}. \tag{30}$$

Similarly for optical phonon deformation potential interaction, the matrix element is derived as [52],

$$|\langle k \pm q|H'_o|k\rangle|^2 = \frac{Z_o^2 \hbar\omega_o}{2V\rho v_s^2}\left(N_q + \frac{1}{2} \pm \frac{1}{2}\right), \tag{31}$$

where Z_o, is the optical deformation potential. Total scattering rate of optical deformation potential (OPD) is relatively easy to calculate,

$$\frac{1}{\tau_{tot}^{opd}} = \sum_{k'} S(k,k'). \tag{32}$$

From Eqs. (15), (31) and (32) we get,

$$\frac{1}{\tau_{tot}^{opd}} = \frac{\pi Z_o^2 \hbar\omega_o N_q}{\hbar V\rho v_s^2}\sum_{k'}\delta(E(k) - E(k') + \hbar\omega). \tag{33}$$

The summation over k' in Eq. (33) is converted into integration while taking care of the fact that electron spin does not change under the interaction.

$$\sum_{k'}\delta(E(k) - E(k') + \hbar\omega) = \frac{V}{2}\int \delta(E - E' + \hbar\omega)g(E')dE' = \frac{Vg(E+\hbar\omega_o)}{2} \tag{34}$$

where g is the density of states given by, for example,

$$g(E) = \frac{1}{L^3}\frac{dN}{dE} = \frac{1}{2\pi^2}\left(\frac{2m^*}{\hbar^2}\right)^{(3/2)}\sqrt{E - E_c}. \tag{35}$$

Now a coupling constant D is introduced as,

$$D^2 = \frac{Z_0^2\omega_0^2}{v_s^2}. \tag{36}$$

The total scattering rate for optical deformation potential scattering becomes, then [52],

$$\frac{1}{\tau_{tot}^{opd}} = \frac{D^2\sqrt{m_l^* m_t^{*2}}}{\sqrt{2}\pi\hbar^3\rho\omega_o}\left[N_q\sqrt{E + \hbar\omega_0} + (N_q + 1)\sqrt{E - \hbar\omega_o}\right]. \tag{37}$$

In order to calculate adsorption and emission probabilities, we define $\lambda_{LO} = \frac{1}{\tau_{LO}^{opd}}$. It is crucial to break Eq. (37) into two parts: absorption rate and emission rate,

$$\lambda_{aLO} = \frac{D^2\sqrt{m_l^* m_t^{*2}}}{\sqrt{2}\pi\hbar^3\rho\omega_o}\left[N_q\sqrt{E + \hbar\omega_0}\right]. \tag{38}$$

$$\lambda_{eLO} = \frac{D^2\sqrt{m_l^* m_t^{*2}}}{\sqrt{2}\pi\hbar^3\rho\omega_o}\left[(N_q + 1)\sqrt{E - \hbar\omega_o}\right]. \tag{39}$$

Now probabilities of an electron to undergo absorption and emission are given by,

$$P_a = \frac{\lambda_{aLO}}{(\lambda_{aLO} + \lambda_{eLO})}, \tag{40}$$

and

$$P_e = \frac{\lambda_{eLO}}{(\lambda_{aLO} + \lambda_{eLO})}, \tag{41}$$

respectively. It is noted that $P_a + P_e = 1$. A random number r is drawn from [0 1]. If $r < P_a$, absorption otherwise emission occurs.

Polar optical phonon (POP) scattering. Electrons can also be scattered by polar optical phonons. This mechanism is dominant in GaN and it is also called polaron scattering. The polar scattering arises from the polarities of the two different atoms in the compound, as illustrated in Fig. (1.b). The total POP scattering rate derived using Fermi-Golden rule is given, straight forward by [53],

$$\lambda_{POP} = \frac{e^2\omega_o\left(\frac{K_0}{K_\infty} - 1\right)}{2\pi K_0\epsilon_0\hbar\sqrt{2\frac{E}{m^*}}}\left[N_q \sinh^{-1}\sqrt{\frac{E}{\hbar\omega_o}} + (N_q + 1)\sinh^{-1}\sqrt{\frac{E}{\hbar\omega_o} - 1}\right], \tag{42}$$

where K_0 is the static dielectric constant, K_∞ is the high frequency dielectric constant, ϵ_0 is the permittivity of free space, N_q is the Bose–Einstein function, $\hbar$ is the plank's constant, E is the electron energy. Absorption and emission rates are obtained separately as,

$$\lambda_{aPOP} = \frac{e^2\omega_o\left(\frac{K_0}{K_\infty} - 1\right)}{2\pi K_0\epsilon_0\hbar\sqrt{2\frac{E}{m^*}}}\left[N_q \sinh^{-1}\sqrt{\frac{E}{\hbar\omega_o}}\right], \tag{43}$$

$$\lambda_{ePOP} = \frac{e^2\omega_o\left(\frac{K_0}{K_\infty} - 1\right)}{2\pi K_0\epsilon_0\hbar\sqrt{2\frac{E}{m^*}}}\left[(N_q + 1)\sinh^{-1}\sqrt{\frac{E}{\hbar\omega_o} - 1}\right], \tag{44}$$

respectively.

Probabilities of emission and absorption are given by,

$$P_a = \frac{\lambda_{aPOP}}{(\lambda_{aPOP} + \lambda_{ePOP})}, \tag{45}$$

$$P_e = \frac{\lambda_{ePOP}}{(\lambda_{aPOP} + \lambda_{ePOP})}. \tag{46}$$

Ionic impurity (IM) scattering. This type of collision is elastic in nature. For an ionized impurity, the scattering source can be characterized by screened Coulomb potential. Typically the ionic impurity density varies between $10^{15} - 10^{17}$ (cm^{-3}). Time dependent perturbation analysis yields the net scattering rate to be [53],

$$\lambda_I = \frac{N_I e^4}{16\sqrt{2m^*}\pi K_0^2\epsilon_0^2}\left[\ln(1+\gamma^2) - \frac{\gamma^2}{1+\gamma^2}\right]E^{-3/2}, \tag{47}$$

where N_I is the impurity density.

$$\gamma = \frac{8m^* E L_D^2}{\hbar^2}, \tag{48}$$

where L_D is the Debye length, given by,

$$L_D = \sqrt{\frac{K_0\epsilon_0 k_b T}{e^2 n_e}}, \tag{49}$$

where n_e is the electron number density, $\frac{1}{\tau_{eI}} = \lambda_I$. The effective relaxation time can be calculated using the Mathissen's rule as,

$$\frac{1}{\tau_e} = \frac{1}{\tau_{eI}} + \frac{1}{\tau_{POP}} + \frac{1}{\tau_{LO}} + \frac{1}{\tau_{LA}}. \tag{50}$$

Mean free path of electrons is calculated using,

$$l_e = v_{th}\tau_e, \tag{51}$$

where v_{th} is the average thermal speed of electrons which is of the order 10^5 (m/s). Based on the relaxation time approximation, the traveling distance of electrons can be obtained by

$$\triangle l_e = l_e \ln(r), \tag{52}$$

where r is a random number.

Electron-LA, electron-LO and electron-POP characterize how effectively the thermal conductivity is influenced by the electrons in GaN. Fig. 2 shows all the four kinds of scattering as a function of electron energy. Among all, POP is found to be the most significant player as seen in Fig. 2. Overwhelming dominance of POP over other EPIs not only reveals the fact that, in what manner the thermal transport is influenced by electrons but also reconfirms the very known polar nature of GaN. Another factor which plays an important role in deciding the impact of EPI is the free electron density. Larger the free electron density stronger the effect of EPI on thermal conductivity. Having said that, Intrinsic GaN has a little free electron concentrations, yet it is found to have a considerable effect on the thermal transport due to its strong polar nature.

2.2.2. Assigning electron properties

It is useful to think of energy band as a collection of discrete energy states. In quantum mechanical terms, each state represents a unique spin (up or down) and a solution to Schrödinger wave equation for periodic potential function. In the conduction band, we get the electron density of states in the final form,

$$g(E) = \frac{8\pi m\sqrt{2m(E - E_c)}}{h^3}, \tag{53}$$

where E_c is the conduction band edge energy.

The probability of state with energy E being occupied by an electron is given by Fermi function

$$f(E) = \frac{1}{1 + e^{\frac{(E-E_f)}{k_B T}}}, \tag{54}$$

where E_f is the Fermi energy. For GaN, intrinsic $E_f = E_g/2$. For extrinsic GaN doped with Si or Ge, E_f moves up towards E_c.

The product $f(E)g(E)dE$ gives the number of electrons per unit volume between E and $E + dE$. Hence, the number of electrons per unit volume in the entire conduction band is given by,

$$n_{De} = \int_{Ec}^{\infty} f(E)g(E)dE. \tag{55}$$

The energy space between E_c and maximum energy is discretized into N_b intervals. The number of electrons in the ith interval is given by,

$$n_i = f_i(E)g_i(E) \triangle E. \tag{56}$$

In order to determine the energy of an electron, a normalized cumulative number density function is first constructed,

$$F_{ei} = \frac{\sum_{k=1}^{i} n_k}{\sum_{k=1}^{N_b} n_k}. \tag{57}$$

A random number r is drawn. If $F_{ei-1} < r < F_{ei}$, the electron is assigned to ith energy interval.

3. Numerical scheme

Boundary scattering mechanisms play an important role in thermal transport. The main boundary conditions of the sample are isothermal at the front and rear ends and adiabatic at the lateral boundaries as we can see in Fig. 3. Isothermal boundaries act like black walls of phonon radiation and they emit or absorb phonons while the adiabatic boundaries simply reflect them. This reflection can be of two types: diffusive or specular. A diffusive parameter d is defined which takes values between 0 and 1. A random number r is drawn and compared

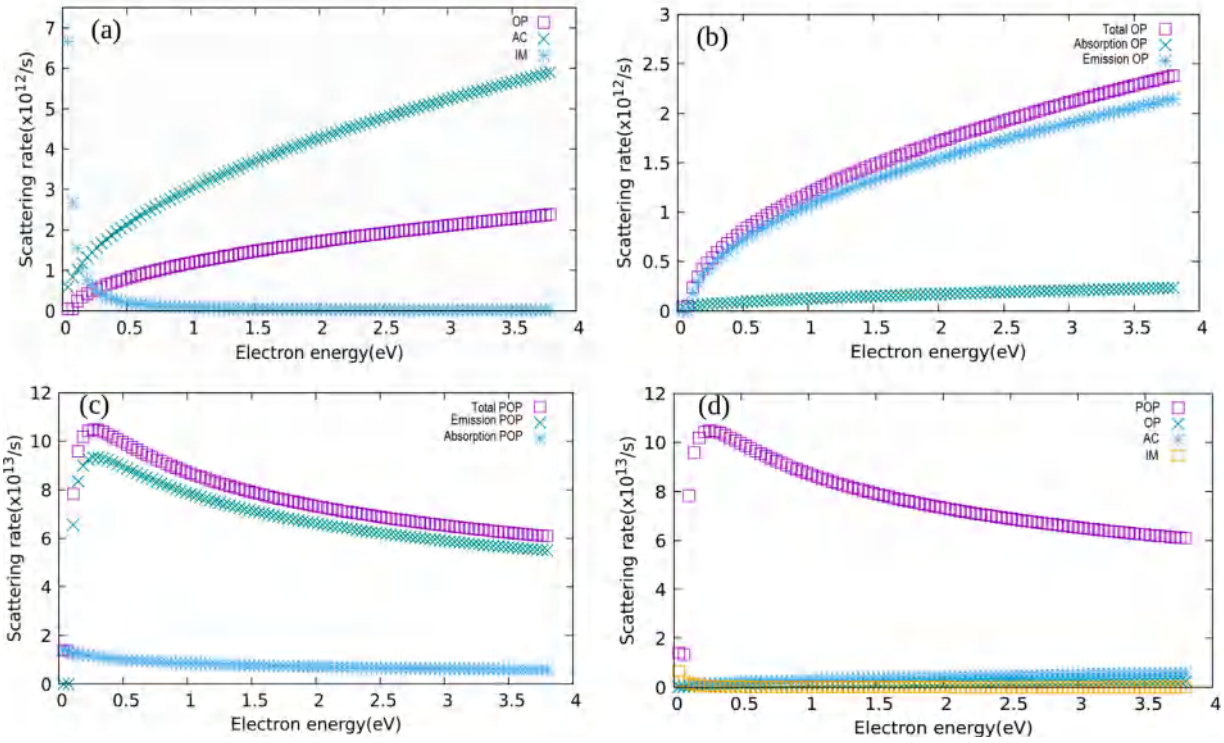

Fig. 2. (a) Electron–impurity (IM)(for impurity density, $N_I = 10^{17}$ cm^{-3}), LA, and LO Scattering are plotted against electron energy. As seen, impurity scattering is dominant for electrons of extremely low energies. (b) Total electron-LO scattering, LO absorption alone and LO emission alone are plotted. Emission is found to be much dominant over absorption for most energy ranges except for low energies. (c) Electron-POP scattering is plotted against electron energy along with its absorption and emission parts. Emission is found be dominating over absorption except for low energies. (d) All POP, LA, LO and IM are plotted together for easy comparison and POP is found to be strongest among all except for low energies.

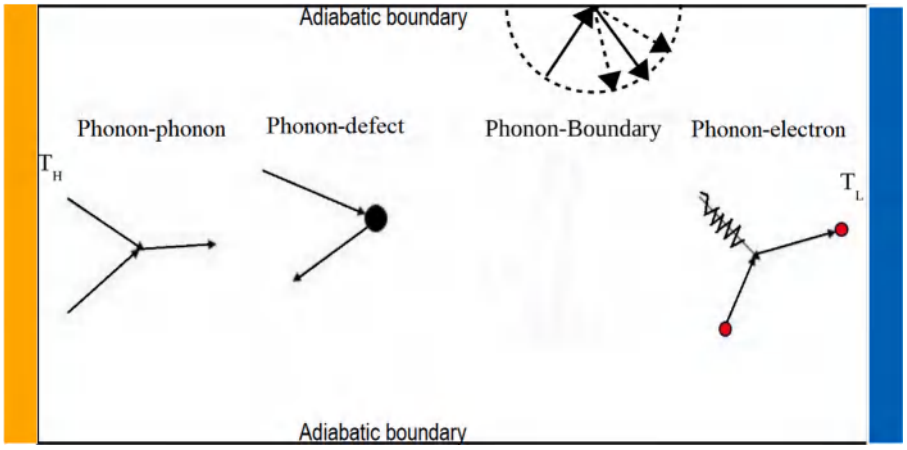

Fig. 3. T_H and T_L are high and low temperatures at two isothermal, front and rear boundaries respectively. Lateral boundaries are shown to be adiabatic.

with d. If $r > d$, the reflection is specular otherwise diffusive. Electron reflections at the boundaries are always taken to be specular. The parameters of GaN used in the computation are acoustic deformation potential Z_A=8.3 eV, optical deformation potential Z_o=4.5 eV, LO phonon frequency ω_o=20 THz [37,54,55].

A detailed flowchart of phonon–electron MC is shown in Fig. 4 which describes the entire process as follows,

1. First, Np the total number of phonon bundles, np the phonon count and ne the electron count are set. Now np is incremented as the first phonon bundle leaves the left boundary. For each phonon bundle, a random position and direction are assigned. A phonon bundle moves interrupted by various scattering processes and ends its trip by getting absorbed by either front or rear boundaries. And entire computational domain is discretized into N_{bin} parallel bins (N_{bin} = 40 for this work), energy is recorded at the bins as the phonon bundles travel by.
2. Once a phonon bundle is absorbed successfully by the boundaries, a factor $t = \frac{n_{De}}{n_{Dp}}$ is introduced, where n_{De} is the electron density and n_{Dp} is the phonon density provided by Eqs. (4) and (55). Electron emission is decided probabilistically i.e. a random number r is compared with t to decide whether to emit electron for each and every phonon emission. Once the electron bundle is emitted, its count, ne is incremented by one. For each electron bundle, a random position and direction are assigned just as in the case of phonon.
3. Electron scattering is chosen probabilistically among LA, LO, IM and POP. In case of LA scattering, LA phonon count is updated in

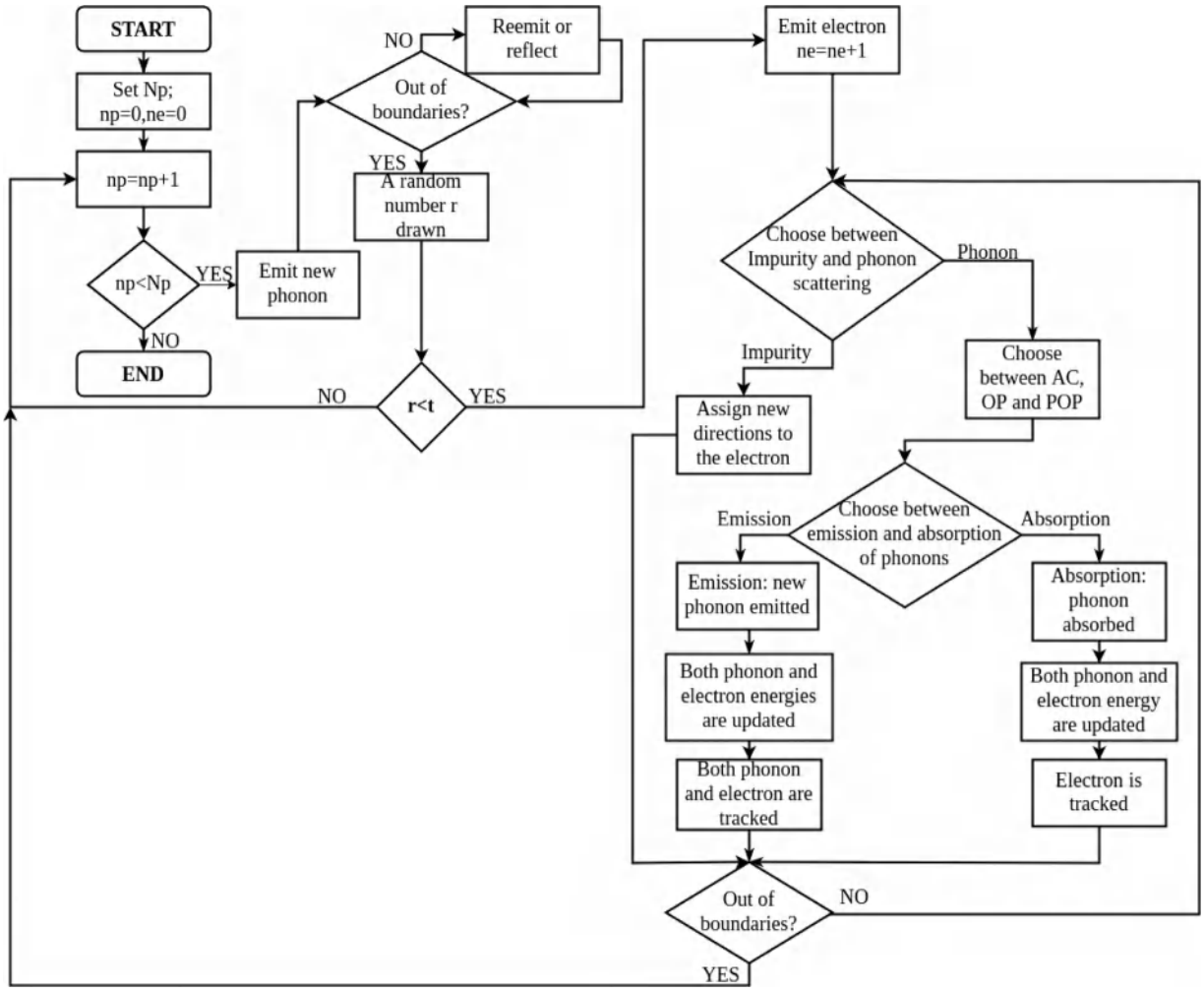

Fig. 4. A flow chart illustrating electron–phonon MC scheme.

the corresponding spacial bin. POP and LO counts are updated by subtracting or adding phonons, depending on whether absorption or emission takes place. In case of emission, the emitted phonon is tracked until it gets absorbed by either of the boundaries and the control is then returned back to the electron that had emitted the phonon and continue its tracking. Energy of the electron is then reduced by that of the emitted phonon and same is added to the corresponding spacial bin, thereby accounting for the energy conservation. If the emitted phonon is of LO branch whose group velocity is marginal, control waits for it to decay into LA/TA phonons whose group velocities are high enough and thus successfully tracked. In case of absorption, electron energy is incremented by that of absorbed phonon and corresponding phonon energy is deducted from the corresponding spacial bin where the absorption had taken placed . The electron alone is then tracked.

4. Once the electron energy becomes weak after continuous interaction (predominantly phonon emission) with phonons, it will be absorbed by the boundaries and the control returns back to step 1. And the entire process repeats again by emitting the next phonon bundle. The lattice temperature profile of the computational domain is first obtained and is used to calculate the temperature gradient and finally the effective thermal conductivity (κ) using the Fourier's relation,

$$\phi = \kappa \frac{dT}{dx}, \tag{58}$$

where ϕ is the heat flux. Electron as well as phonon bundle populations at three different spatial bins(x=25 nm, x=250 nm and x=500 nm) can be seen in Fig. 5. Both electron and phonon populations are found to be increasing linearly with respect to the number of iterations.

4. Results and discussion

The temperature distribution inside the material is an important aspect which plays a key role in thermal conductivity calculation, yet most of experimental techniques are unable to determine it directly. MC method, however, gives an elaborate picture of how temperature is distributed inside nanostructures under heat transport. Phonon temperature at each spacial bin is defined using the pseudo temperature relation [23],

$$E_T w_{ph} = \sum_p \sum_{i=1}^{i=N_b} \frac{\hbar\omega_i D(\omega_i, p)\Delta\omega_i}{\exp[\hbar\omega_i / k_B T_{ph}] - 1}, \tag{59}$$

where E_T is the target energy of a spacial bin. Assuming thermodynamic equilibrium at each and every spacial bins, thus calculated pseudo temperature is close to thermodynamic temperature of the system. Fig. (6.a) gives the temperature profile of GaN films of 500 nm thickness, both for with EPI and without EPI scenarios. Temperature as a function of distance is found to be linear with a negative slope, highest at the left boundary (T_H), tapering linearly towards the left boundary (T_L). With EPI temperature is found to be little elevated with

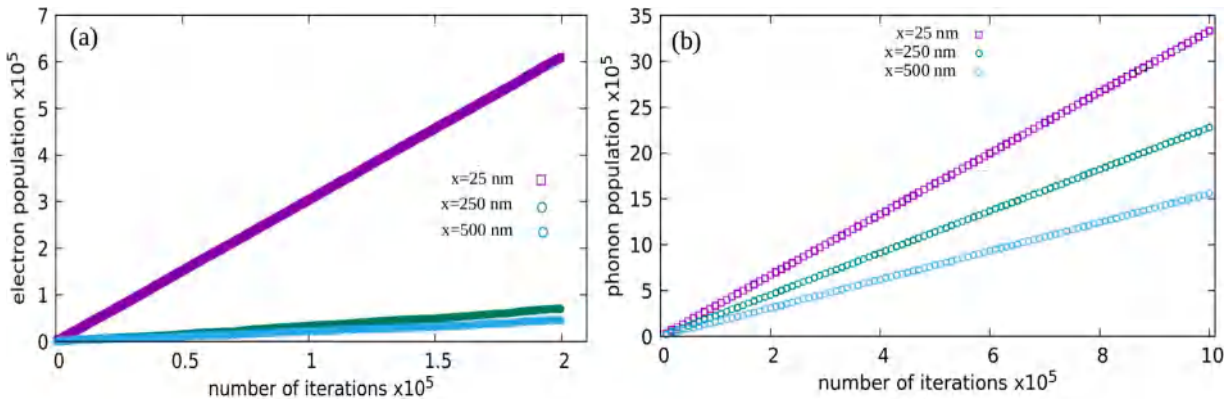

Fig. 5. (a) Electron bundle population versus number of iterations for $x = 25$ nm, 250 nm and 500 nm. The real electron population can be obtained by multiplying electron bundle population with certain weighting factor w_e used to cut down the computational expenses (b) Phonon bundle population versus number of iterations for $x = 25$ nm, 250 nm and 500 nm. The real Phonon population can be obtained by multiplying Phonon bundle population with certain weighting factor w_{ph} used to cut down the computational expenses.

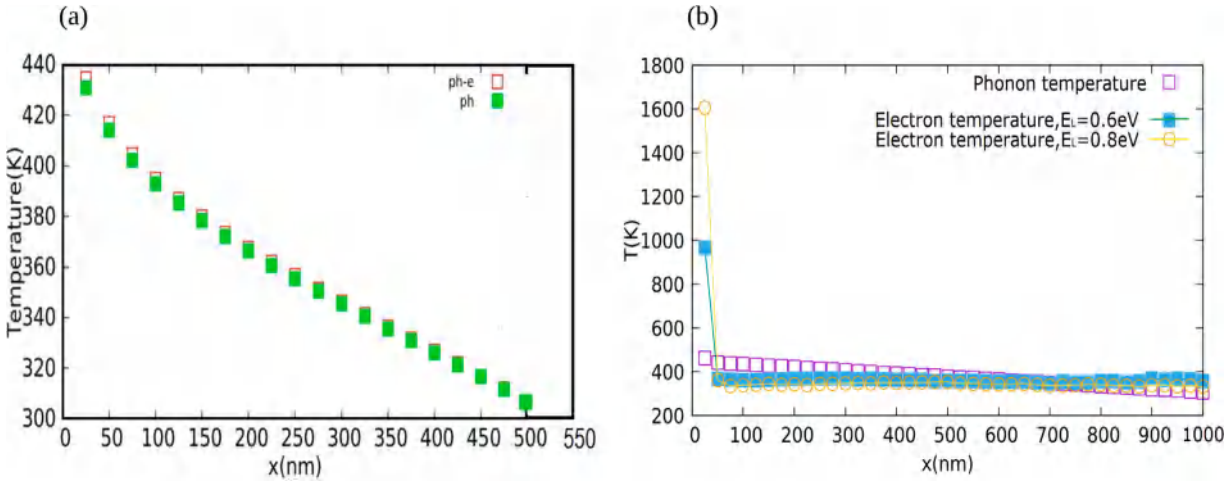

Fig. 6. (a) Temperature plotted against distance, for sample length $L_x = 500$ nm. "ph" and "ph-e" stand for without EPI and with EPI respectively. (b) Electron temperature for left boundary electron energy, $E_L = 0.6$ eV and 0.8 eV plotted along with phonon temperature under EPI for comparison.

respect to that without EPI. The difference is more noticeable close to the left/high temperature boundary and becomes irrelevant as the distance increases, towards the right/low temperature boundary. This is because, the energetic electrons emitted from left are rapidly losing their energy by means of EPI due to the fact that the electron mean free path is of order 1–10 nm, much smaller than that of phonons. Consequently, EPI influences the temperature profile, therefore affecting the temperature gradient which is one of the key factors deciding the lattice thermal conductivity. Another important parameter, which determines the thermal conductivity, the heat flux is also affected by electron–phonon interaction due to the number of phonons added by the electrons as they travel through the material. Electron temperature in the computational domain is defined using the relation in Ref. [27]:

$$\frac{3}{2}k_B T_{ei} = f\left(\frac{1}{2}m^* < v >_i^2 - \frac{1}{2}m^* v_d^2\right), \tag{60}$$

where f, m^*, $< v >_i^2$, and v_d refer to the electron fraction, effective mass, mean-square velocity, and drift velocity respectively with the underlying assumption that the external applied field is zero and thereby the drift velocity is negligibly small. Here T_{ei} is the electron temperature for ith bin. A plot of T_e along with lattice temperature is shown in the Fig. (6.b). As we can see, the temperature of electrons entering the left high temperature boundary is decayed rapidly, as the electrons interact with phonons by significantly transferring their energy to phonons. And it is important to note that, though the electron temperature and lattice temperature at the left boundary are far apart, as the electrons travel through the domain, they lose energy and thereby eventually the electron temperature approaches the lattice temperature. Nevertheless, electron temperatures are not included in the lattice thermal conductivity calculation. The length scale at which the electron temperature catch up with the lattice temperature is found to be of order equal to the average electron mean free path. We remark that the electron temperature defined thusly is not identical to the true or thermodynamic temperature of the electron ensemble. For electron concentrations in the degenerate range, the temperature as given above exceeds the true temperature of the electron ensemble because the Pauli exclusion principle limits the number of low-energy particles in the ensemble, consequently raising the average energy of the ensemble. Therefore, it is better to state that the above defined electron temperature is more likely a reflection of the average energy of electron bundle. The electrons originating from the left boundary of the computational domain are set to have a maximum energy, E_L. An electron temperature vs distance plot for E_L=0.6 eV and E_L=0.8 eV is shown in Fig. (6.b)

Categories of EPI scattering have been studied are electron-longitudinal acoustic (LA), electron longitudinal optical (LO) and electron polar optical phonon (POP) to characterize the electronic influence

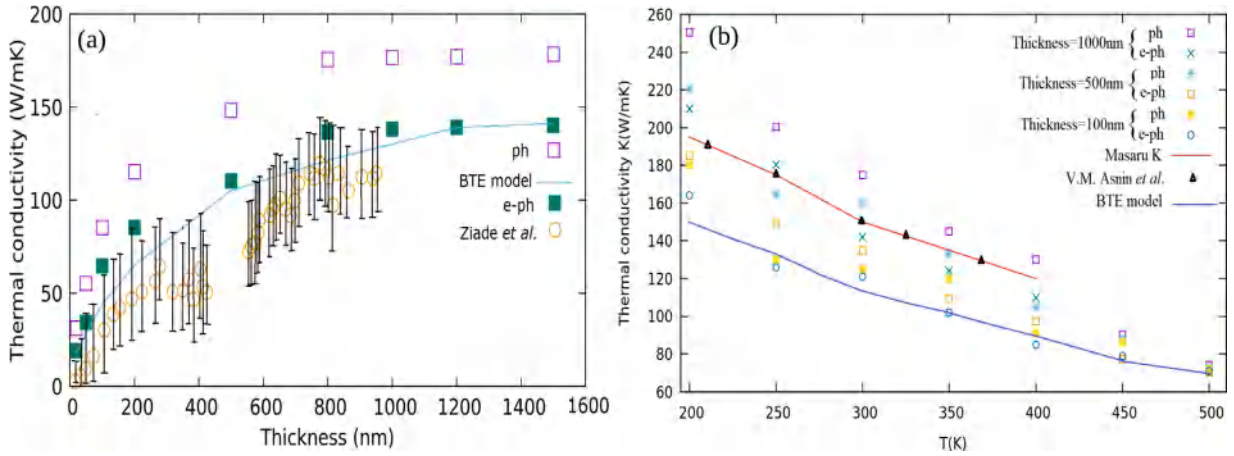

Fig. 7. (a) Thermal conductivity vs thickness plot where "ph" and "e-ph" stand for without EPI and with EPI scenarios respectively, the experimental study by Elbara Ziad et al. [41] and a BTE model [41] also can be seen. (b) Thermal conductivity vs Temperature, present work for sample thicknesses 100 nm, 500 nm and 1000 nm, a few past studies [39,40] and a BTE model [41] for comparison.

of heat transport in GaN. Among all, POP is found to be the dominant player as seen in Fig. 2. Moreover, mostly, the phonon emission probabilities are much stronger than their absorption counterparts because electron energies are much higher when compared with that of phonons. Therefore, electrons are more likely to lose energy by emitting phonons than to gain energy by absorbing phonons. As we can see in Fig. 2 absorption rates are higher than emission rates only when the electron energies fall below phonon energies from then electrons start absorbing more phonons thereby gaining energy. More and more phonons added by electrons, due to emission processes, into the GaN lattice eventually dissipate more heat into the bulk of the material, thus reducing the heat conduction significantly. Consequently, the lattice thermal conductivity of wurtzite GaN at room temperatures is found to be reduced by 16%–22% for samples of varying thicknesses. The sample thickness is successfully varied from 10 nm to 1500 nm. The effect of EPI on thermal conductivity is found to be slightly more pronounced for smaller thicknesses. The thermal conductivity vs thickness is compared with a BTE model used in Ref. [41] and found to be in a good agreement with it as seen in Fig. (7.a). Thermal conductivity (K) vs thickness is found to be in a good agreement with a work by Elbara Ziade et al. [41] as well, within a discrepancy limit of 2%–4%. Lattice thermal conductivity and EPI vs temperature is studied for a range 200 K to 500 K for sample lengths of 100 nm, 500 nm and 1000 nm and are compared with a work by Kamano et al. [39], Asnin et al. [40] and a BTE model used in Ref. [41]. Thermal conductivity vs temperature is found to have good agreement with BTE model and other studies for the given range of temperatures as shown in Fig. (7.b). EPI influence on thermal conductivity is found to be more pronounced near room temperature and weakening at high temperatures.

5. Conclusions

Heat conduction in micro/nano-scale materials are effectively described by Boltzmann transport equation. The Monte Carlo method is an efficient computational tool for solving BTE statistically. In summary, we have developed a novel MC algorithm which combines phonon and electron transport strategically to address electron–phonon interactions. Both phonons and electrons are injected into the computational domain from the hot end and the motion is tracked considering all types of scattering which they undergo through. The process is repeated till an ensemble of trajectories is formed. Initial phonon and electron properties are assigned using the schemes described in Sections 2.1 and 2.2 respectively. Different scattering mechanisms of both phonons and electrons are incorporated. Overall the present method is found to be adept in dealing with energy transfer between electrons and phonons.

Electron–phonon MC is applied in a case study, simulating the thermal transport in wurtzite Gallium Nitride (GaN), considering EPI impact into account. Deformation potential as well as polar optical potential were used to characterize EPI. Both lattice temperature and the electron temperature profiles in the computational domain were estimated and compared. While the lattice temperature profile was found to be linear the electron temperature depicted a strong non-linear behavior. The electron temperature was found to be decaying rapidly thus catching up with the lattice temperature. The length scale at which the electron temperature catch up with the lattice temperature was estimated to be very close to the average electron mean free path. The lattice temperature profile was found to be modified by EPI, degree of which is more near the left boundary and almost ceases to exist near the right boundary. This is because, the high energy electrons emitted from left loses the energy rapidly as they travel so electrons with very little energy are found near the right boundary. The number of phonons emitted by the electrons also influence the heat flux. Both these mechanisms caused a reduction in the thermal conductivity. The inference is that the lattice thermal conductivity of wurtzite GaN at room temperature is found to be reduced by 16%–22%, after incorporating EPI, for samples of varying thicknesses. Among all EPIs the POP is found to be the most dominant player verifying the strong polar nature of GaN. We used the novel MC to study the thermal transport in a GaN film of thickness range of 10–1000 nm and data showed good agreement with the BTE model and some past studies. The investigation on thermal conductivity vs temperature was also found to be in good agreement with a BTE model. These results may be useful for engineering future generations of wide-band gap semiconductor devices like GaN/AlGaN High mobility electron transistors. Our investigation provides a deep insight into the role of electron–phonon coupling in thermal transport in wurtzite GaN and the understanding gained from this work is expected to stimulate future studies of similar phenomenon in other polar semiconductors. Since the method combines both phonon MC and electron MC together, it may be more suitable to study heat transport properties and electron transport properties like, drift velocity, carrier mobility etc. simultaneously.

Declaration of competing interest

The authors declare that they have no known competing financial interests or personal relationships that could have appeared to influence the work reported in this paper.

Data availability

Data will be made available on request.

Acknowledgments

This work was supported by National Natural Science Foundation of China (Grant Nos: 51825601, U20A20301).

References

[1] J.M. Ziman, Electrons and Phonons: The Theory of Transport Phenomena in Solids, Oxford University Press, Oxford, New York, 2001.
[2] L. Lindsay, First principles peierls-boltzmann phonon thermal transport: a topical review, Nanoscale Microscale Thermophys. Eng. 20 (2) (2016) 67, http://dx.doi.org/10.1080/15567265.2016.1218576.
[3] T. Feng, X. Ruan, Higher-order phonon scattering: Advancing the quantum theory of phonon linewidth, thermal conductivity and thermal radiative properties, in: Nanoscale Energy Transport: Emerging Phenomena, Methods and Applications, first ed., IOP Publishing, Bristol, UK, 2020.
[4] A.J. Minnich, et al., Thermal conductivity spectroscopy technique to measure phonon mean free paths, Phys. Rev. Lett. 107 (9) (2011) 095901, http://dx.doi.org/10.1103/PhysRevLett.107.095901.
[5] C. Hua, Phonon mean free path spectroscopy: Theory and experiments, in: Nanoscale Energy Transport: Emerging Phenomena, Methods and Applications, first ed., IOP Publishing, Bristol, UK, 2020.
[6] B. Liao, et al., Significant reduction of lattice thermal conductivity by the electron–phonon interaction in silicon with high carrier concentrations: a first-principles study, Phys. Rev. Lett. 114 (11) (2015) 115901, http://dx.doi.org/10.1103/PhysRevLett.114.115901.
[7] A. Sommerfeld, H. Bethe, Handbuch Der Physik, Vol. XXIV, Springer, Berlin, 1933, p. 33.
[8] R.E.B. Makinson, The thermal conductivity of metals, Math. Proc. Camb. Phil. Soc. 34 (1938) 474.
[9] F. Bloch, Über die Quantenmechanik der Elektronen in Kristallgittern, Z. Phys. 52 (7–8) (1929) 555, http://dx.doi.org/10.1007/BF01339455.
[10] D.A. Broido, M. Malorny, G. Birner, N. Mingo, D.A. Stewart, Intrinsic lattice thermal conductivity of semiconductors from first principles, Appl. Phys. Lett. 91 (2007) 231922.
[11] K. Esfarjani, G. Chen, H.T. Stokes, Heat transport in silicon from first-principles calculations, Phys. Rev. B 84 (8) (2011) 085204, http://dx.doi.org/10.1103/PhysRevB.84.085204.
[12] F. Giustino, M.L. Cohen, S.G. Louie, Electron–phonon interaction using wannier functions, Phys. Rev. B 76 (16) (2007) 165108, http://dx.doi.org/10.1103/PhysRevB.76.165108.
[13] Z. Tong, S. Li, X. Ruan, H. Bao, Comprehensive first principles analysis of phonon thermal conductivity and electron–phonon coupling in different metals, Phys. Rev. B 100 (14) (2019) 144306, http://dx.doi.org/10.1103/PhysRevB.100.144306.
[14] Ankit Jain, Alan J.H. McGaughey, Thermal transport by phonons and electrons in aluminum, silver, and gold from first principles, Phys. Rev. B 93 (2016) 081206(R).
[15] Yu-Chao Hua, Bing-Yang Cao, Phonon ballistic-diffusive heat conduction in silicon nanofilms by Monte Carlo simulations, Int. J. Heat Mass Transfer 78 (2014) 755–759.
[16] J.D. Albrecht, R.P. Wang, P.P. Ruden, M. Farahmand, K.F. Brennan, Monte Carlo calculation of electron transport properties of bulk AlN, J. Appl. Phys. 83 (1998) 1446, http://dx.doi.org/10.1063/1.366848.
[17] B. Gelmont, K. Kim, M. Shur, Monte Carlo simulation of electron transport in gallium nitride, J. Appl. Phys. 74 (1993) 1818, http://dx.doi.org/10.1063/1.354787.
[18] Ján Kolník, İsmail H. Oğuzman, Kevin F. Brennan, Rongping Wang, P. Paul Ruden, Yang Wang, Electronic transport studies of bulk zincblende and wurtzite phases of GaN based on an ensemble Monte Carlo calculation including a full zone band structure, J. Appl. Phys. 78 (1995) 1033, http://dx.doi.org/10.1063/1.360405.
[19] Enrico Bellotti, Bhautik K. Doshi, Kevin F. Brennan, John D. Albrecht, P. Paul Ruden, Ensemble Monte Carlo study of electron transport in wurtzite InN, J. Appl. Phys. 85 (1999) 916, http://dx.doi.org/10.1063/1.369211.
[20] Jean-Philippe M. Peraud, Nicolas G. Hadjiconstantinou, An alternative approach to efficient simulation of micro/nanoscale phonon transport, Appl. Phys. Lett. 101 (2012) 153114, http://dx.doi.org/10.1063/1.4757607.
[21] Yunfei Chen, Deyu Li, Arun Majumdar, Monte Carlo simulation of silicon nanowire thermal conductivity, J. Heat Transfer 127 (10) (2005) 1129–1137, http://dx.doi.org/10.1115/1.2035114.
[22] Dao-Sheng Tang, Yu-Chao Hua, Bing-Yang Cao, Thermal wave propagation through nanofilms in ballistic-diffusive regime by Monte Carlo simulations, Int. J. Therm. Sci. 109 (2016) 81–89.
[23] Sandip Mazumder, Arunava Majumdar, Monte Carlo study of phonon transport in solid thin films including dispersion and polarization, J. Heat Transfer 123 (4) (2001) 749–759, http://dx.doi.org/10.1115/1.1377018.
[24] Jaona Randrianalisoa, Dominique Baillis, Monte Carlo simulation of steady-state microscale phonon heat transport, J. Heat Transfer 130 (7) (2008) 072404, http://dx.doi.org/10.1115/1.2897925.
[25] D. Baillis, J. Randrianalisoa, Prediction of thermal conductivity of nanostructures: Influence of phonon dispersion approximation, Int. J. Heat Mass Transfer 52 (2009) 2516–2527, http://dx.doi.org/10.1016/j.ijheatmasstransfer.2009.01.017.
[26] C. Jacoboni, L. Reggiani, The Monte Carlo method for solution of charge transport in semiconductor with application to covalent materials, Rev. Modern Phys. 55 (1983) 645–705.
[27] Udayan V. Bhapkar, Michael S. Shur, Monte Carlo calculation of velocity-field characteristics of wurtzite GaN, J. Appl. Phys. 82 (1997) 1649, http://dx.doi.org/10.1063/1.365963.
[28] T. Klitsner, J.E. VanCleve, H.E. Fisher, R.O. Pohl, Phonon radiative heat transfer and surface scattering, Phys. Rev. B 38 (1988) 7576–7594.
[29] R.B. Peterson, Direct simulation of phonon-mediated heat-transfer in a debye crystal, J. Heat Transfer 118 (1994) 815–822.
[30] S.V.J. Narumanchi, J.Y. Murthy, C.H. Amon, Submicron heat transport model in silicon accounting for phonon dispersion and polarization, J. Heat Transfer 126 (2004) 946–955.
[31] X.L. Nguyen, T.N.N. Nguyen, B.T. Chau, M.C. Dang, The fabrication of GaN-based light emitting diodes (LEDs), Adv. Nat. Sci.: Nanosci. Nanotechnol. 1 (2010) 025015.
[32] N. Han, T.V. Cuong, M. Han, B.D. Ryu, S. Chandramohan, J.B. Park, J.H. Kang, Y.J. Park, K.B. Ko, H.Y. Kim, H.K. Kim, J.H. Ryu, Y.S. Katharria, C.-J. Choi, C.-H. Hong, Improved heat dissipation in gallium nitride light-emitting diodes with embedded graphene oxide pattern, Nature Commun. 4 (2013) 1452.
[33] L. Lindsay, D.A. Broido, T.L. Reinecke, Ab initio thermal transport in compound semiconductors, Phys. Rev. B 87 (2013) 165201, 10.
[34] D.A. Broido, M. Malorny, G. Birner, N. Mingo, D.A. Stewart, Intrinsic lattice thermal conductivity of semiconductors from first principles, Appl. Phys. Lett. 91 (2007) 231922.
[35] L. Lindsay, D.A. Broido, T.L. Reinecke, Thermal conductivity and large isotope effect in GaN from first principles, Phys. Rev. Lett. 109 (2012) 095901.
[36] Dao-Sheng Tang, Guang-Zhao Qin, Ming Hu, Thermal transport properties of GaN with biaxial strain and electron–phonon coupling, J. Appl. Phys. 127 (2020) 035102, http://dx.doi.org/10.1063/1.5133105.
[37] Jia-Yue Yang, Guangzhao Qin, Ming Hu, Nontrivial contribution of Fröhlich electron–phonon interaction to lattice thermal conductivity of wurtzite GaN, Appl. Phys. Lett. 109 (2016) 242103.
[38] Guangzhao Qin, Zhenzhen Qin, Huimin Wang, Ming Hu, Anomalously temperature-dependent thermal conductivity of monolayer GaN with large deviations from the traditional 1/T law, Phys. Rev. B 95 (2017) 195416.
[39] Masaru Kamano, Masanobu H. Araguchi, Takahiro N. Iwaki, Masuo F. Ukui, Minoru K. Uwahara, Toshihiro O. Kamoto, Takashi M. Ukai, Temperature dependence of the thermal conductivity and phonon scattering time of a bulk GaN crystal, Jpn. J. Appl. Phys. 41 (2002).
[40] V.M. Asnin, F.H. Pollak, J. Ramer, M. Schurman, I. Ferguson, High spatial resolution thermal conductivity of lateral epitaxial overgrown GaN/sapphire (0001) using a scanning thermal microscope, Appl. Phys. Lett. 75 (1999) 1240.
[41] Elbara Ziade, Jia Yang, Gordie Brummer, Denis Nothern, Theodore Moustakas, Aaron J. Schmidt, Thickness dependent thermal conductivity of gallium nitride, Appl. Phys. Lett. 110 (2017) 031903, http://dx.doi.org/10.1063/1.4974321.
[42] C. Mion, Y.C. Chang, J.F. Muth, P. Rajagopal, J.D. Brown, Thermal conductivity of GaN grown on silicon substrates, in: Mat. Res. Soc. Symp. Proc. Vol. 798 ©2004 Materials Research Society.
[43] Takahiro Kawamura, Yoshihiro Kangawa, Koichi Kakimoto, Investigation of thermal conductivity of GaN by molecular dynamics, J. Cryst. Growth 284 (2005) 197–202.
[44] X.W. Zhou, S. Aubry, R.E. Jones, A. Greenstein, P.K. Schelling, Towards more accurate molecular dynamics calculation of thermal conductivity. Case study: GaN bulk crystals, 2021, arxiv:1206.5445v1 [cond-mat.mtr1-sci].
[45] Qiye Zheng, Chunhua Li, Akash Rai, Jacob H. Leach, David A. Broido, David G. Cahill, Thermal conductivity of GaN, and SiC from 150 K to 850 K, Phys. Rev. Mater. 3 (2019) 014601.
[46] C. Luo, D.R. Clarke, J.R. Dryden, The temperature dependence of the thermal conductivity of single crystal GaN films, Electron. Mater. 30 (3) (2001) 138.
[47] N. Ashcroft, N. Mermin, Solid State Physics, international ed., Saunders College, Philiadelphia, 1976.
[48] J.D. Chung, A.J.H. McGaughey, M. Kaviany, Role of phonon dispersion in lattice thermal conductivity modeling, J. Heat Transfer 126 (2004) 376–380.
[49] M.G. Holland, Analysis of lattice thermal conductivity, Phys. Rev. 132 (1963) 2461–2471.
[50] K.T. Tsen, D.K. Ferry, S.M. Goodnick, A. Salvador, H. Morkoc, Decay of the longitudinal optical phonons in wurtzite GaN and $Al_xGa_{1-x}N$, Physica B 272 (1999) 406–408.
[51] B.K. Ridley, The LO phonon lifetime in GaN, J. Phys.: Condens. Matter 8 (1996) L511.
[52] K. Hess, Advanced Theory of Semiconductor Devices, first ed., Wiley, 1999, pp. 94–95.

[53] Mark Lundstrom, Fundamentals of Carrier Transport, second ed., Cambridge UNIVERSITY PRESS, 2000.

[54] I. Vurgaftman, J.R. Meyer, Band parameters for nitrogen-containing semiconductors, J. Appl. Phys. 94 (2003) 3675, http://dx.doi.org/10.1063/1.1600519.

[55] Qimin Yan, Patrick Rinke, Matthias Scheffler, Chris G. Van de Walle, Strain effects in group-III nitrides: Deformation potentials for AlN, GaN, and InN, Appl. Phys. Lett. 95 (2009) 121111.